Research Article | Vol. 25, No. 17 | 21 Aug 2017 | OPTICS EXPRESS 19832

Optics EXPRESS

Generalized optical angular momentum sorter and its application to high-dimensional quantum cryptography

HUGO LAROCQUE,[1] JÉRÉMIE GAGNON-BISCHOFF,[1] DOMINIC MORTIMER,[1] YINGWEN ZHANG,[1] FRÉDÉRIC BOUCHARD,[1] JEREMY UPHAM,[1] VINCENZO GRILLO,[2] ROBERT W. BOYD,[1,3] AND EBRAHIM KARIMI[1,4,*]

[1]*Department of Physics, University of Ottawa, 25 Templeton St., Ottawa, Ontario, K1N 6N5 Canada*
[2]*CNR-Istituto Nanoscienze, Centro S3, Via G Campi 213/a, I-41125 Modena, Italy*
[3]*Institute of Optics, University of Rochester, Rochester, New York 14627, USA*
[4]*Department of Physics, Institute for Advanced Studies in Basic Sciences, 45137-66731 Zanjan, Iran*
[*]*ekarimi@uottawa.ca*

Abstract: The orbital angular momentum (OAM) carried by optical beams is a useful quantity for encoding information. This form of encoding has been incorporated into various works ranging from telecommunications to quantum cryptography, most of which require methods that can rapidly process the OAM content of a beam. Among current state-of-the-art schemes that can readily acquire this information are so-called OAM *sorters*, which consist of devices that spatially separate the OAM components of a beam. Such devices have found numerous applications in optical communications, a field that is in constant demand for additional degrees of freedom, such as polarization and wavelength, into which information can also be encoded. Here, we report the implementation of a device capable of sorting a beam based on its OAM and polarization content, which could be of use in works employing both of these degrees of freedom as information channels. After characterizing our fabricated device, we demonstrate how it can be used for quantum communications via a quantum key distribution protocol.

OCIS codes: (230.3720) Liquid-crystal devices; (260.6042) Singular optics; (270.5568) Quantum cryptography.

References and links

1. H. Rubinsztein-Dunlop, A. Forbes, M. Berry, M. R. Dennis, D. L. Andrews, M. Mansuripur, C. Denz, C. Alpmann, P. Banzer, T. Bauer, E. Karimi, L. Marrucci, M.J. Padgett, M. Ritsch-Marte, N. M. Litchinitser, N. P. Bigelow, C. Rosales-Guzmán, A. Belmonte, J. P. Torres, T. W. Neely, M. Baker, R. Gordon, A. Stilgoe, J. Romero, A. G. White, R. Fickler, A. E. Willner, G. Xie, B. McMorran, and A. M. Weiner, "Roadmap on structured light," J. Opt. **19**(1), 013001 (2016).
2. L. Allen, M. W. Beijersbergen, R. Spreeuw, and J. Woerdman, "Orbital angular momentum of light and the transformation of laguerre-gaussian laser modes," Phys. Rev. A **45**(11), 8185 (1992).
3. M. Krenn, R. Fickler, M. Fink, J. Handsteiner, M. Malik, T. Scheidl, R. Ursin, and A. Zeilinger, "Communication with spatially modulated light through turbulent air across vienna," New J. Phys. **16**(11), 113028 (2014).
4. J. Wang, J.-Y. Yang, I. M. Fazal, N. Ahmed, Y. Yan, H. Huang, Y. Ren, Y. Yue, S. Dolinar, M. Tur, and A. E. Willner, "Terabit free-space data transmission employing orbital angular momentum multiplexing," Nat. Photon. **6**(7), 488–496 (2012).
5. A. E. Willner, H. Huang, Y. Yan, Y. Ren, N. Ahmed, G. Xie, C. Bao, L. Li, Y. Cao, Z. Zhao, J. Wang, M. P. J. Lavery, M. Tur, S. Ramachandran, A. F. Molisch, N. Ashrafi, and S. Ashrafi, "Optical communications using orbital angular momentum beams," Adv. Opt. Photon. **7**(1), 66–106 (2015).
6. F. Tamburini, E. Mari, A. Sponselli, B. Thidé, A. Bianchini, and F. Romanato, "Encoding many channels on the same frequency through radio vorticity: first experimental test," New J. Phys. **14**(3), 033001 (2012).
7. A. Sit, F. Bouchard, R. Fickler, J. Gagnon-Bischoff, H. Larocque, K. Heshami, D. Elser, C. Peuntinger, K. Günthner, B. Heim, C. Marquardt, G. Leuchs, R. W. Boyd, and E. Karimi, "High-dimensional intra-city quantum cryptography with structured photons," arXiv preprint arXiv:1612.05195 (2016).
8. G. Vallone, V. D'Ambrosio, A. Sponselli, S. Slussarenko, L. Marrucci, F. Sciarrino, and P. Villoresi, "Free-space quantum key distribution by rotation-invariant twisted photons," Phys. Rev. Lett. **113**(6), 060503 (2014).
9. G. C. Berkhout, M. P. Lavery, J. Courtial, M. W. Beijersbergen, and M. J. Padgett, "Efficient sorting of orbital angular momentum states of light," Phys. Rev. Lett. **105**(15), 153601 (2010).

#295105 https://doi.org/10.1364/OE.25.019832
Journal © 2017 Received 3 May 2017; revised 24 Jun 2017; accepted 24 Jul 2017; published 7 Aug 2017

Optics EXPRESS

10. M. N. O'Sullivan, M. Mirhosseini, M. Malik, and R. W. Boyd, "Near-perfect sorting of orbital angular momentum and angular position states of light," Opt. Express **20**(22), 24444–24449 (2012).
11. M. Mirhosseini, M. Malik, Z. Shi, and R. W. Boyd, "Efficient separation of the orbital angular momentum eigenstates of light," Nat. Commun. **4**, 2781 (2013).
12. M. P. Lavery, D. J. Robertson, G. C. Berkhout, G. D. Love, M. J. Padgett, and J. Courtial, "Refractive elements for the measurement of the orbital angular momentum of a single photon," Opt. Express **20**(3), 2110–2115 (2012).
13. M. Mirhosseini, O. S. Magaña-Loaiza, M. N. O'Sullivan, B. Rodenburg, M. Malik, M. P. J. Lavery, M. J. Padgett, D. J. Gauthier, and R. W. Boyd, "High-dimensional quantum cryptography with twisted light," New J. Phys. **17**, 033033 (2015).
14. V. Grillo, A. H. Tavabi, F. Venturi, H. Larocque, R. Balboni, G. C. Gazzadi, S. Frabboni, P.-H. Lu, E. Mafakheri, F. Bouchard, R. E. Dunin-Borkowski, R. W. Boyd, M. P. J. Lavery, M. J. Padgett, and E. Karimi, "Measuring the orbital angular momentum spectrum of an electron beam," Nat. Commun. **8**, 15536 (2017).
15. B. J. McMorran, T. R. Harvey, and M. P. Lavery, "Efficient sorting of free electron orbital angular momentum," New J. Phys. **19**(2), 023053 (2017).
16. S. Pancharatnam, "Generalized theory of interference and its applications," Proc. Indian Acad. Sci. A **44**(6), 398–417 (1956).
17. M. V. Berry, "Quantal phase factors accompanying adiabatic changes," Proc. R. Soc. A **392**(1802), 45–57 (1984).
18. L. Marrucci, C. Manzo, and D. Paparo, "Pancharatnam-berry phase optical elements for wave front shaping in the visible domain: Switchable helical mode generation," Appl. Phys. Lett. **88**(22), 221102 (2006).
19. Z. Bomzon, V. Kleiner, and E. Hasman, "Pancharatnam–berry phase in space-variant polarization-state manipulations with subwavelength gratings," Opt. Lett. **26**(18), 1424–1426 (2001).
20. L. Marrucci, C. Manzo, and D. Paparo, "Optical spin-to-orbital angular momentum conversion in inhomogeneous anisotropic media," Phys. Rev. Lett. **96**(16), 163905 (2006).
21. E. Nagali, F. Sciarrino, F. De Martini, L. Marrucci, B. Piccirillo, E. Karimi, and E. Santamato, "Quantum information transfer from spin to orbital angular momentum of photons," Phys. Rev. Lett. **103**(1), 013601 (2009).
22. L. Marrucci, E. Karimi, S. Slussarenko, B. Piccirillo, E. Santamato, E. Nagali, and F. Sciarrino, "Spin-to-orbital conversion of the angular momentum of light and its classical and quantum applications," J. Opt. **13**(6), 064001 (2011).
23. E. Karimi, J. Leach, S. Slussarenko, B. Piccirillo, L. Marrucci, L. Chen, W. She, S. Franke-Arnold, M. J. Padgett, and E. Santamato, "Spin-orbit hybrid entanglement of photons and quantum contextuality," Phys. Rev. A **82**(2), 022115 (2010).
24. G. F. Walsh, "Pancharatnam-berry optical element sorter of full angular momentum eigenstate," Opt. Express **24**(6), 6689–6704 (2016).
25. H. Larocque, J. Gagnon-Bischoff, F. Bouchard, R. Fickler, J. Upham, R. W. Boyd, and E. Karimi, "Arbitrary optical wavefront shaping via spin-to-orbit coupling," J. Opt. **18**(12), 124002 (2016).
26. W. Hossack, A. Darling, and A. Dahdouh, "Coordinate transformations with multiple computer-generated optical elements," J. Mod. Opt. **34**(9), 1235–1250 (1987).
27. E. Karimi, B. Piccirillo, L. Marrucci, and E. Santamato, "Light propagation in a birefringent plate with topological charge," Opt. Lett. **34**(8), 1225–1227 (2009).
28. V. Chigrinov, A. Muravski, H. S. Kwok, H. Takada, H. Akiyama, and H. Takatsu, "Anchoring properties of photoaligned azo-dye materials," Phys. Rev. E **68**(6), 061702 (2003).
29. S. Nersisyan, N. Tabiryan, D. M. Steeves, and B. R. Kimball, "Fabrication of liquid crystal polymer axial waveplates for uv-ir wavelengths," Opt. Express **17**(14), 11926–11934 (2009).
30. H. Wu, W. Hu, H.-c. Hu, X.-w. Lin, G. Zhu, J.-W. Choi, V. Chigrinov, and Y.-q. Lu, "Arbitrary photo-patterning in liquid crystal alignments using dmd based lithography system," Opt. Express **20**(15), 16684–16689 (2012).
31. J. Kim, Y. Li, M. N. Miskiewicz, C. Oh, M. W. Kudenov, and M. J. Escuti, "Fabrication of ideal geometric-phase holograms with arbitrary wavefronts," Optica **2**(11), 958–964 (2015).
32. M. N. Miskiewicz and M. J. Escuti, "Direct-writing of complex liquid crystal patterns," Opt. Express **22**(10), 12691–12706 (2014).
33. T.-C. Poon and T. Kim, *Engineering Optics with MATLAB*® (World Scientific Publishing Co Inc, 2006).
34. C. H. Bennett and G. Brassard, "Quantum cryptography: Public key distribution and coin tossing," Theor. Comput. Sci. **560**, 7–11 (2014).
35. P. W. Shor and J. Preskill, "Simple proof of security of the BB84 quantum key distribution protocol," Phys. Rev. Lett. **85**(2), 441 (2000).
36. Y. Guo, M. Jiang, C. Peng, K. Sun, O. Yaroshchuk, O. Lavrentovich, and Q.-H. Wei, "High-resolution and high-throughput plasmonic photopatterning of complex molecular orientations in liquid crystals," Adv. Mater. **28**(12) 2353–2358 (2016).
37. L. A. Romero and F. M. Dickey, "Theory of optimal beam splitting by phase gratings. I. one-dimensional gratings," J. Opt. Soc. Am. A **24**(8), 2280–2295 (2007).
38. D. Prongué, H.-P. Herzig, R. Dändliker, and M. T. Gale, "Optimized kinoform structures for highly efficient fan-out elements," Appl. Opt. **31**(26), 5706–5711 (1992).
39. L. De Sio, D. E. Roberts, Z. Liao, S. Nersisyan, O. Uskova, L. Wickboldt, N. Tabiryan, D. M. Steeves, and B. R. Kimball, "Digital polarization holography advancing geometrical phase optics," Opt. Express **24**(16), 18297–18306

Optics EXPRESS

(2016).
40. S. R. Nersisyan and N. V. Tabiryan, "Polarization imaging components based on patterned photoalignment," Mol. Cryst. Liq. Cryst. **489**(1), 156–482 (2008).
41. N. V. Tabiryan, S. V. Serak, D. E. Roberts, D. M. Steeves, and B. R. Kimball, "Thin waveplate lenses of switchable focal length-new generation in optics," Opt. Express **23**(20), 25783–25794 (2015).
42. N. V. Tabiryan, S. V. Serak, S. R. Nersisyan, D. E. Roberts, B. Y. Zeldovich, D. M. Steeves, and B. R. Kimball, "Broadband waveplate lenses," Opt. Express **24**(7), 7091–7102 (2016).
43. E. Karimi, S. A. Schulz, I. De Leon, H. Qassim, J. Upham, and R. W. Boyd, "Generating optical orbital angular momentum at visible wavelengths using a plasmonic metasurface," Light Sci. Appl. **3**(5), e167 (2014).
44. D. Lin, P. Fan, E. Hasman, and M. L. Brongersma, "Dielectric gradient metasurface optical elements," Science **345**(6194), 298–302 (2014).
45. Y. S. Rumala, G. Milione, T. A. Nguyen, S. Pratavieira, Z. Hossain, D. Nolan, S. Slussarenko, E. Karimi, L. Marrucci, and R. R. Alfano, "Tunable supercontinuum light vector vortex beam generator using a q-plate," Opt. Lett. **38**(23), 5083–5086 (2013).
46. G. Milione, M. P. Lavery, H. Huang, Y. Ren, G. Xie, T. A. Nguyen, E. Karimi, L. Marrucci, D. A. Nolan, R. R. Alfano, and A. E. Willner, "4× 20 Gbit/s mode division multiplexing over free space using vector modes and a q-plate mode (de) multiplexer," Opt. Lett. **40**(9), 1980–1983 (2015).

1. Introduction

The panoply of means for distinctively shaping light beams has significantly improved the performance of applications such as optical tweezers and communications, while also driving their usage in emerging fields like quantum cryptography [1]. Such advancements can be attributed to the several degrees of freedom that are used to characterize an optical beam, such as its wavelength, temporal profile, transverse spatial profile, and its polarization, which can often be naturally extended to the quantum description of light beams. For instance, a photon's angular momentum, which includes spin angular momentum (SAM) and orbital angular momentum (OAM), is one such property. SAM is attributed to a beam's polarization, which is associated with the vectorial nature of light, whereas OAM is related to the beam's transverse phase profile. Namely, beams that carry ℓ units of OAM are characterized by an azimuthally dependent phase defined by an $\exp(i\ell\varphi)$ term in their formulation, where φ is the transverse azimuthal coordinate [2]. Consequently, their wavefronts consist of ℓ intertwined helices. Among the distinguishing features of OAM-carrying beams is the fact that they are orthogonal to one another and are thus of significant interest in optical communications, where information is encoded into a single photon's OAM [3–6], sometimes in conjunction with another optical degree of freedom like polarization [7, 8]. In practice, these methods aim to increase the rate at which information can be transferred and have thus motivated the development of several schemes that can readily acquire an optical beam's OAM content. Much like how polarizing beam splitters can split a beam's orthogonally polarized components, some of these schemes include devices that spatially separate a beam based on its OAM composition [9]. These so-called OAM *sorters* have been granted a significant amount of attention as indicated by works that have improved their efficiencies [10, 11] and their scalability [12] along with those that have extended their applications to fields ranging from quantum communications [13] to electron microscopy [14, 15]. OAM sorters primarily rely on the use of two confocal phase elements that are often implemented by means of spatial light modulators (SLM) [9]. The phase added by the latter is essentially based on a transverse modulation of the optical path length experienced by the beam's cross-section. Other types of phase modulating mechanisms could also be employed for this purpose such as those that impart a geometric phase [16, 17] to a beam. Such phases are added by means of Pancharatnam-Berry optical phase elements (PBOE), which are able to add tailored yet opposite phases to a beam's circularly polarized components accompanied by a flip in their handedness [18, 19]. This process inevitably introduces a relation between a beam's spatial profile and its polarization, and hence constitutes a form of spin-to-orbit coupling [20], which has been heavily investigated in the framework of quantum information [21–23].

Recently, a theoretical proposal introduced a PBOE-based OAM sorter that exploits this

Optics EXPRESS

relation with the beam's polarization as a means of additionally sorting optical SAM states [24]. Here, we report the implementation of such a generalized optical angular momentum sorter where we employ custom-made liquid crystal devices [25] as the required PBOEs. This PBOE sorting scheme experiences less losses and is more compact than those based on SLMs while also being able to modulate an optical beam's transverse phase profile based on its polarization. We characterize our sorter by feeding it with beams carrying well-defined values of OAM and circular polarizations. Afterwards, we verify that the sorter functions for beams consisting of superpositions of such states, and we evaluate the device's crosstalk. Finally, we test the device's performance in the single-photon regime and use it in an OAM-based quantum key distribution (QKD) protocol.

2. Theory

An OAM sorter's performance primarily relies on the unwrapping of a beam's azimuthal phase variations into variations along a Cartesian coordinate [9]. In the case of an OAM-carrying beam, its unwrapped form will consist of tilted wavefronts whose tilt is proportional to the beam's original OAM value. When made to propagate through a lens, these tilted waves will focus at different positions, thus enabling the spatial separation of a beam based on its original OAM content. In practice, the unwrapping crucial to this process is achieved by means of a conformal mapping between Cartesian (x, y) and scaled log-polar $(u = -a\ln(\sqrt{x^2+y^2}), v = a\arctan(y/x))$ coordinates, where a and b are scaling parameters. This transformation can be realized by using the following confocal phase elements [26]:

$$\text{Unwrapper}: \ \phi_1(x,y) = \frac{2\pi a}{\lambda f}\left[y\arctan\left(\frac{y}{x}\right) - x\ln\left(\frac{\sqrt{x^2+y^2}}{b}\right) + x\right] \tag{1}$$

$$\text{Corrector}: \ \phi_2(u,v) = -\frac{2\pi ab}{\lambda f}\exp\left(-\frac{u}{a}\right)\cos\left(\frac{v}{a}\right), \tag{2}$$

where λ is the wavelength of the beam and f is the focal length of the lens used to perform the mapping. Specifically, the ϕ_1 element performs the required unwrapping while the ϕ_2 element provides the final phase corrections to the beam in order to complete the mapping. These elements will hereafter be referred to as the *unwrapper* and the *corrector* elements, respectively.

Using PBOEs as the sorter's phase elements introduces a polarization-dependent transformation onto the beam [27]. This polarization dependence is attributed to the fact that PBOEs are birefringent devices characterized by a spatially varying optical axis. When these are tuned to half-wave optical retardation, the handedness of the SAM components is flipped and the beam gains a Pancharatnam-Berry (geometric) phase due to the distribution of the device's optical axis [18]. More specifically, a PBOE defined by an optical axis distribution of $\alpha(x_1, x_2)$, where x_1 and x_2 are transverse coordinates, will add a phase of $\pm 2\alpha(x_1, x_2)$ on left-right–handed circularly polarized light, respectively, accompanied by a flip in the handedness of these circular polarizations.

In cases where this polarization inversion occurs, a beam going through a PBOE defined by an optical axis of $\alpha = \phi_1/2$ will cause any right-handed circularly polarized light to undergo a reversed unwrapping process with respect to the conventional one experienced by left-handed circularly polarized light, thus enabling a spatial separation between both of the unwrapped circularly polarized components. Given that the beam's original right-handed circular polarization now unwraps at the horizontal position $u_R = -u_L$, where u_L is the conventional unwrapped position taken by the left-handed circular polarization, the sorter's second element must be modified accordingly to provide the required phase corrections to both of the beam's polarization components [24]. Therefore, to provide a proper phase correction to the unwrapped beam [26], u is replaced by $-|u|$ in Eq. (2) and is multiplied by a factor of -1 to account for polarization-

Optics EXPRESS

dependent effects, i.e. $\tilde{\phi}_2(u,v) = \frac{2\pi ab}{\lambda f}\exp\left(\frac{|u|}{a}\right)\cos\left(\frac{v}{a}\right) - \frac{\pi}{\Lambda}u$, where the additional grating term $(\pi/\Lambda)u$ is added to provide further separation between both polarizations upon propagation through the sorter's second lens [24]. The separation of these two orthogonally polarized components enabled by the first PBOE thereby allows for a device capable of sorting optical angular momentum eigenstates and, in turn, of handling an increased amount of information channels that can be used in practical applications.

3. Fabrication

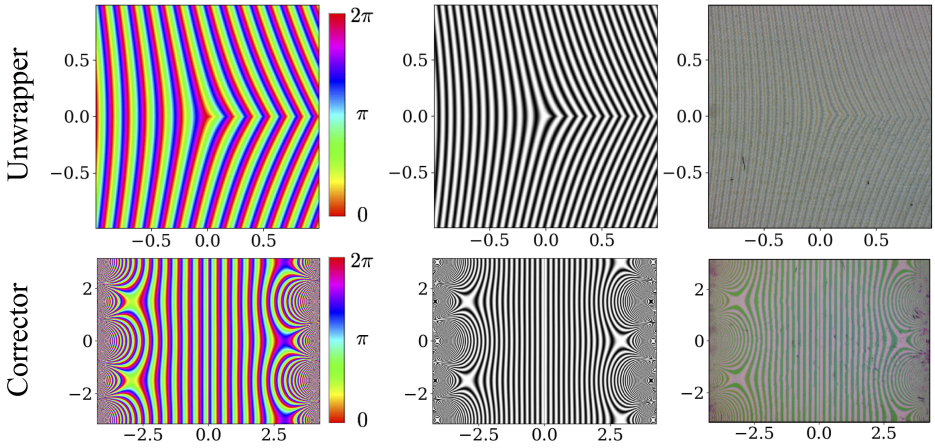

Fig. 1. The geometric phase 2α (left) attributed to the unwrapper (top) and corrector (bottom) elements; (center) the devices' expected transmission when placed between two polarizers; (right) the devices' observed transmission patterns. The axes' units are in mm.

Our sorter's implementation relies on the use of custom-made liquid crystal devices as the required PBOEs [25]. These devices consist of a layer of patterned 6CHBT nematic liquid crystals confined within two indium tin oxide (ITO)-coated substrates separated by spacer-grade silica microspheres. The substrates are additionally spin-coated with a layer of azobenzene-based dye molecules [28,29]. We specifically use microspheres with a diameter below 4.8 μm and the azobenzene-based aligning material PAAD-22 provided by BEAM Co. The orientation of the liquid crystals is determined by that of the dye molecules which are aligned by means of a photo-alignment method used to reconstruct the device's desired optical axis distribution [25,30–32]. To fabricate the PBOEs required to perform the sorting process, we adapted such a photo-alignment method to produce liquid crystal devices with an optical axis distribution defined by $\alpha_1 = \phi_1/2$ and $\alpha_2 = \tilde{\phi}_2/2$. The sorting parameters that appear in ϕ_1 and $\tilde{\phi}_2$ were chosen to optimize the sorter's performance without significantly compromising the quality of the fabricated elements. That being said, we used parameters of $a = 3/(2\pi)$ mm, $b = 2$ μm, $\lambda = 810$ nm, $f = 500$ mm, and $\Lambda = 200$ μm. These parameters can also be optimized for other wavelengths including those that are commonly used in telecommunications. The corresponding geometric phase 2α attributed to the element along with the device's expected and observed appearance between two crossed polarizers are shown in Fig. 1. The close resemblance of these patterns suggests that the unwrapper and corrector have been fabricated with reasonable fidelity to the design.

Our devices have an efficiency of 72%. Most losses however occur due to reflections from their cells' glass substrates. These losses can be eliminated by means of an anti-reflection coating to increase their efficiency to a value closer to their conversion efficiency, which can realistically

Optics EXPRESS

reach values of 97% [25]. To ensure that our devices operate at the half-wave condition required to perform the sorting process, we also soldered wires on the conductive side of their ITO substrates. This addition allows us to apply a tuning voltage to the device which modifies the birefringence of our device's liquid crystals. Minor errors in the fabrication process introduced some aberrations in the devices as later shown in experimental results. We attribute the latter to a minor scaling error in our photo-alignment. This displaces the region where the unwrapped beam hits the corrector element, thus preventing the completion of the conformal mapping required to perform the sorting process. To overcome this issue, we shifted our beam's wavelength until its unwrapped components interacted with the regions of the corrector that enabled an optimal phase correction while simultaneously tuning our device's half-wave retardation to the examined wavelength. We found that this optimal wavelength was 850 nm and thereby employed this value in our experiments.

4. Results

We characterized our device using the experimental setup shown in Fig. 2, which allows us to provide several types of optical beams to the sorter. We first examined the sorter's output when

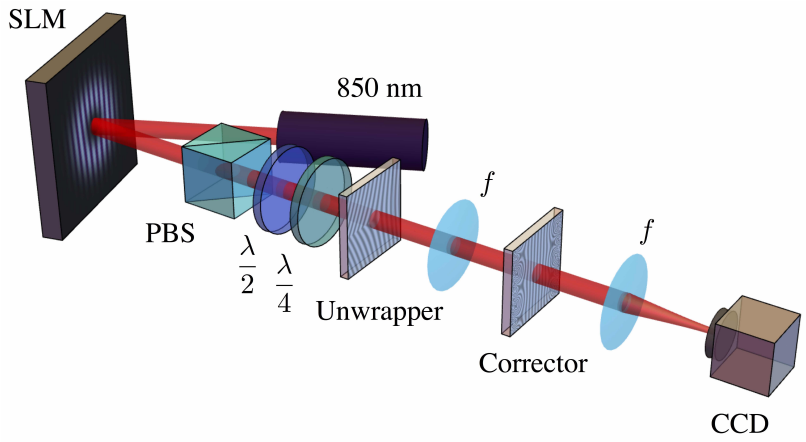

Fig. 2. Experimental setup used to characterize the sorter. A spatial light modulator (SLM) is used to provide a distinct phase and intensity profile to a beam coming from a 850 nm diode laser while a set of elements composed of a polarizing beamsplitter (PBS), a half-wave plate ($\lambda/2$), and a quarter-wave plate ($\lambda/4$) is used to provide the beam with a specific polarization. The beam then goes through the sorter which consists of the unwrapper PBOE, a lens, the corrector PBOE, and another lens. The sorter's output is then examined with a CCD camera.

fed with circularly polarized beams carrying well-defined OAM values and compared it with simulated outputs obtained using the split-step beam propagation method [33]. Such beams will hereafter be referred to as optical angular momentum eigenstates. The intensity profile of the sorted beams are shown in Fig. 3(a). We can observe that the sorted orders attributed to left- and right-handed circularly polarized light are clearly distinguishable from one another while simultaneously exhibiting good separation between the conventional OAM orders attributed to the confocal phase elements. Moreover, we also note that the transverse positions of the right-handed circular OAM orders are inverted with respect to those of the left-handed circular ones, thus verifying that these two polarizations do indeed acquire opposite phases as they propagate through the sorter. Minor effects attributed to the device's aberrations are also noticeable most notably by the lower definition of the experimental sorted orders when compared with the

Optics EXPRESS

simulated output of an ideal sorter shown in Fig. 3(b). This lower definition is also observed in Fig. 3(c) where we show the simulated profile of a beam going through an aberrated sorter. The latter namely consists of elements with phase patterns compressed by a factor of 4% which accounts for the scaling errors in the device's fabrication. Nevertheless, the lower order modes depicted in Fig. 3(a) are sufficiently distinct for practical applications as further demonstrated.

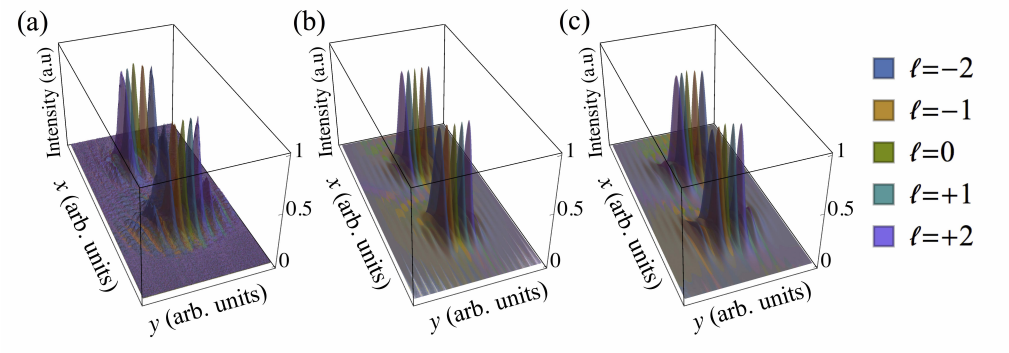

Fig. 3. Relative intensity profiles of the sorter's output when fed with circularly polarized beams defined by OAM values ranging from $\ell = -2$ to $\ell = 2$. (a) Measured output of the fabricated sorter. (b) Simulated output of a perfect sorter. (c) Simulated output of an aberrated sorter. Left-handed circular polarizations appear at the bottom of the plots while right-handed circular polarizations appear at the top.

Following this first calibration process, we tested our sorter's performance for beams consisting of a superposition of angular momentum eigenstates. Such a superposition can consist of a circularly polarized beam in a superposition of OAM states, an OAM state in a superposition of polarization states (i.e. a non-circularly polarized beam) or a combination of the two. We demonstrate these three cases in Fig. 4, where we can observe the sorter's performance for all types of superpositions. Once again, we show our experimental results, the simulated output of the ideal sorter, and the simulated output of the aberrated sorter in Fig. 4(a)-(c), respectively. The device's limitations at higher absolute OAM values is clearly observed in the far-right column of Fig. 4, where we provide the sorted orders for the case of linearly polarized light in a superposition of $\ell = +2$ and $\ell = -2$ states. The line appearing between the two orders of the far-right column of Fig. 4(a),(c) clearly indicates the less-defined nature of higher order modes which start to spread out over transverse positions attributed to other modes, e.g. the $\ell = 0$ mode in this case.

In order to further examine the effects related to the overlap of the sorted orders, we evaluated the crosstalk between the modes shown in Fig. 3. To do so, we assigned an elliptically shaped channel to each mode based on the data shown in Fig. 3 and computed the relative intensity of each mode in these channels. These relative intensities can be found in Fig. 5. Our experimental results shown in Fig. 5(a) indicate that 72% of the intensity of a given angular momentum state is found in its respective channel which is comparable to the simulated value of 75% for an aberrated sorter based on the data shown in Fig. 5(c). Both of these quantities are lower than the optimal values of 89% attributed to a perfect sorter whose results are displayed in Fig. 5(b). When adapted to the sorting parameters of previously implemented sorters, this optimal value agrees with those obtained from simulations in earlier works [9]. Though the fact that we are using different sorting parameters prevents us from directly comparing our device's experimental crosstalk with those of other OAM sorters, we do observe that the latter have a similar difference between numerical and experimental crosstalk values [9]. This similarity thereby establishes

Optics EXPRESS

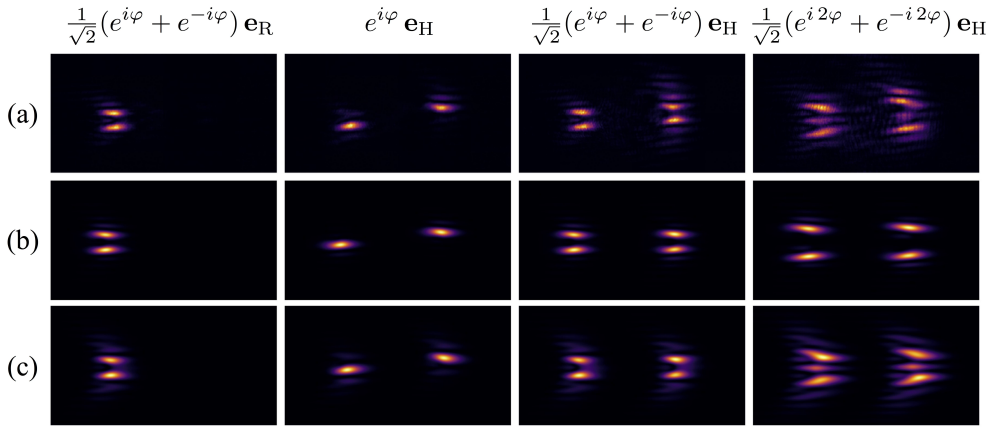

Fig. 4. Relative intensity profiles of the sorter's output when fed with a selection of superpositions of beams consisting of different circular polarizations and OAM values ranging from $\ell = -2$ to $\ell = 2$ for (a) experimental results, (b) simulated results attributed to a perfect sorter, and (c) simulated results attributed to an aberrated sorter. Here $\mathbf{e}_{\mathrm{L}}$ and $\mathbf{e}_{\mathrm{R}}$ correspond to the left- and right-handed circular polarization vectors, respectively, and $\mathbf{e}_{\mathrm{H}} = (\mathbf{e}_{\mathrm{L}} + \mathbf{e}_{\mathrm{R}})/\sqrt{2}$ is the horizontal polarization vector.

that our sorter's performance is experimentally comparable to that of its OAM counterpart. For practical purposes however, this percentage can be slightly raised, at the expense of decreasing the device's efficiency, by reducing the size of the channels attributed to each OAM value.

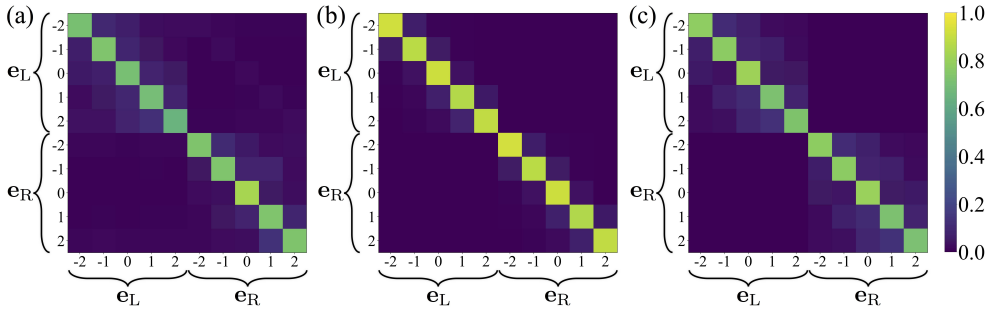

Fig. 5. Relative intensities of angular momentum states found in each angular momentum channel for (a) experimental results, (b) simulated optimal results, and (c) simulated results for an aberrated sorter. We considered states defined by left- and right-handed circular polarizations and by OAM states ranging from $\ell = -2$ to $\ell = 2$.

As mentioned earlier, one of the most attractive features of optical angular momentum states is their natural extension to the quantum nature of light which makes them of interest in quantum communications. Given that our device preserves coherence [21], we examined its performance in the single photon regime for photons in optical angular momentum eigenstates $|\pi, \ell\rangle$ where π and ℓ are states defining the photon's polarization and OAM, respectively. This was achieved by using a pair of down-converted photons generated through spontaneous parametric down-conversion by pumping a ppKTP crystal with 405 nm UV light. The first of the two was sent

Optics EXPRESS

through the sorter and later detected by an ICCD camera which was triggered by the second photon. The resulting images are shown in Fig. 6 along with their classical counterparts. We can observe a good agreement between the images taken in the classical and quantum regimes, thus verifying our device's performance at the single photon level.

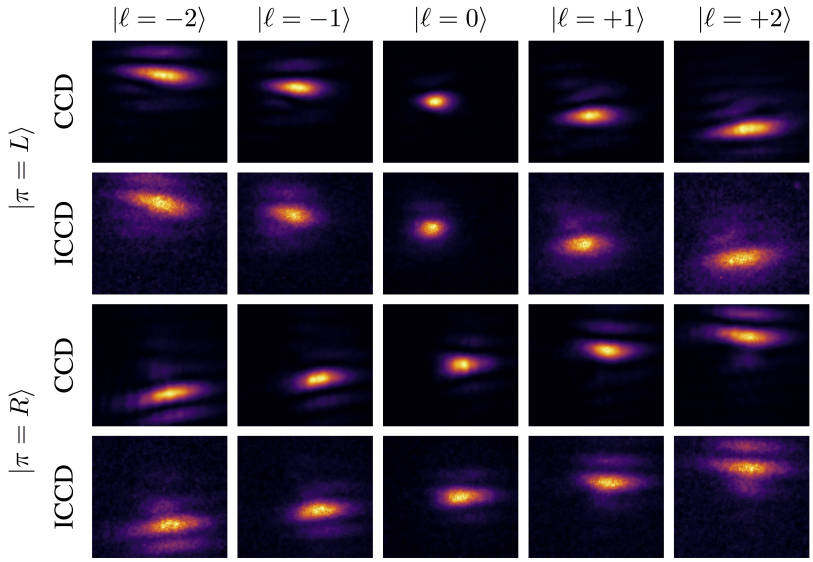

Fig. 6. The sorter's output when fed with single photons in angular momentum eigenstates. The images were taken using a triggered ICCD camera. The images are grouped with their classical counterparts which correspond to ones taken with a regular CCD camera with coherent light going through the sorter.

Now that we have established that our sorter exhibits a satisfactory level of crosstalk along with a good performance with single photons, we proceed by demonstrating how our device can be employed in a practical application. More specifically, we test our sorter for high-dimensional quantum cryptography given the extensive body of works exploring the use of OAM sorters in this field [11,13]. In particular, we perform a high-dimensional extension of the seminal quantum key distribution BB84 protocol [34], the former of which has been recognized to securely transmit an increased amount of information. In the first place, for the case of an error-free quantum channel, Alice, the sender, may send a total of $\log_2(d)$ bits of information per photon, where d is the dimensionality of the protocol, to Bob, the receiver, hence increasing the overall secure key rate. Moreover, it is well-known that QKD protocols may be performed only up to a certain error threshold. In the case of the standard 2-dimensional BB84, this error threshold is given by 11.0%, where no secret shared key may be established beyond this level of error. However, by increasing the dimensionality of the BB84 protocol, this error threshold may be increased, e.g. in the case of $d = 10$ the error threshold is given by 26.2% [35]. Therefore, higher-dimensional QKD extensions are much more robust to noise and device imperfections. Most of the works on high-dimensional QKD revolve around an OAM based QKD protocol where the employed mutually unbiased bases consist of quantum states that can be spatially separated using a sorter. This sorter, however, is differently configured to perform measurements in each of these bases. That being said, the first basis used in this scheme usually consists of the OAM basis whose states can be readily measured using the conventional sorter configuration depicted in Fig. 2. The states $|\ell\rangle$ of this basis usually range from OAM values of $\ell = -N$ to $\ell = N$, and hence the dimensionality of $d = 2N + 1$. The second basis corresponds to the so-called angular basis whose states can

Optics EXPRESS

be expressed in terms of the OAM basis as $|n\rangle_{\text{ang}} = d^{-1/2} \sum_{\ell=-N}^{N} \exp(i\,2\pi n\ell/d)\,|\ell\rangle$ [11, 13], where n is an integer between $-N$ and N. In addition to being mutually unbiased with respect to OAM modes, angular modes are defined by distinct angular shaped intensity profiles that nearly do not overlap with one another. Therefore, because they are already spatially separated, they consist of the perfect complementary basis for performing QKD with OAM-carrying beams. Though a measurement in the angular basis could in principle be performed on the beam without manipulating it, such a measurement is often configured by using the unfocused output of the sorter which essentially consists of the unwrapped beam where the angular modes occupy distinct transverse positions as opposed to angular ones. Such a configuration is usually employed in order to enable the use of secondary methods aiming to reduce the crosstalk between these unwrapped modes. With these factors in consideration, a BB84 QKD protocol relying on these two mutually unbiased bases consists of Alice randomly generating states belonging to these two bases and sending them to Bob that randomly performs a measurement in either of these bases using his two different sorter configurations. Using our sorter, we expand on this scheme by using

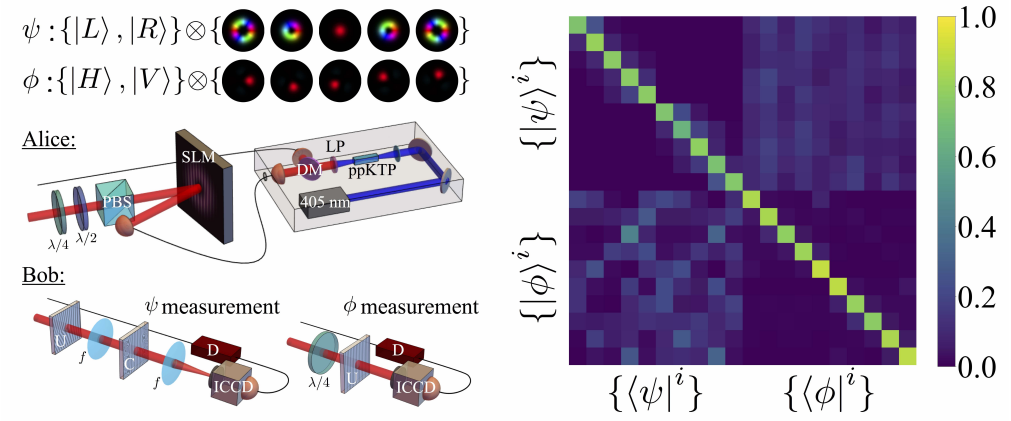

Fig. 7. Summary of the QKD demonstration conducted with our generalized angular momentum sorter. Top left: Mutually unbiased bases ψ and ϕ used in this demonstration where states attributed to spatial modes are depicted as their transverse phase profile in hue colours masked by their intensity profile. Bottom left: setups used by Alice and Bob in this QKD scheme. Alice's state preparation setup randomly generates a state either in the ψ or ϕ basis using an SLM, a quarter-wave plate ($\lambda/4$), a half-wave plate ($\lambda/2$), and a PBS. The single photons that she uses come from a down converted 405 nm source consisting of a pair of 850 nm and 775 nm photons. The latter are separated using a dichroic mirror (DM) thus enabling the use of the 850 nm photon as the *signal* photon and the 775 nm one as the *idler* photon. Bob then randomly performs a measurement in either the ψ or ϕ basis using two different sorter configurations and an ICCD camera that is triggered by the *idler* photon using a detector (D). Right: Probability-of-detection matrix of our QKD scheme. Figure legend: ppKTP = periodically-poled KTP crystal, LP=long-pass filter, U=unwrapper, C=corrector.

a single photon's polarization to increase the size of these mutually unbiased bases by a factor of two. Namely, the OAM basis $\{|-N\rangle, , |N\rangle\}$ is now extended to the generalized optical angular momentum basis $\psi = \{|L\rangle, |R\rangle\} \otimes \{|-N\rangle, , |N\rangle\}$, where $|L\rangle$ and $|R\rangle$ respectively correspond to left- and right-handed circularly polarized states, and now consists of the optical angular momentum eigenstates that have been discussed in this work. As in the case of our classical measurements, single photon measurements in the optical angular momentum basis can be carried out using the sorter configuration depicted in Fig. 2. As for the complementary basis, we chose $\phi = \{|H\rangle, |V\rangle\} \otimes \{|-N\rangle_{\text{ang}}, , |N\rangle_{\text{ang}}\}$, which corresponds to the product of the angular basis

Optics EXPRESS

$\{|-N\rangle_{\text{ang}}, , |N\rangle_{\text{ang}}\}$ with the polarization basis consisting of horizontally $|H\rangle$ and vertically $|V\rangle$ polarized states, both of which are unbiased with respect to their angular momentum counterparts. To perform a measurement in this basis, we first make our single photons go through a quarter-wave plate in order to map horizontally and vertically polarized states to left- and right-handed polarized ones. After this, the photons go through a region of the unwrapper element that is far from its centre and that closely resembles a grating. This process enables the separation of angular modes in the $\{|H\rangle, |V\rangle\}$ basis, and thus a measurement in the complementary ϕ basis given that angular modes inherently exhibit good spatial separation. A summary of this scheme along with experimental results are shown in Fig. 7, where we conducted such a protocol defined by a $N = 2$ parameter, thus enabling 10-dimensional quantum key distribution. In a d-dimensional BB84 protocol, the secret key rate is given by $R = \log_2(d) - 2h^{(d)}(e_b)$, where $h^{(d)}(x) := -x\log_2(x/(d-1)) - (1-x)\log_2(1-x)$ is the d-dimensional Shannon entropy. Here, we obtained a quantum bit error rate of $e_b = 21.2\%$, corresponding to a secret key rate of $R = 0.49$ bits/photon. These values are directly limited by our device's crosstalk, which, as we mentioned above, is significantly increased by its aberrations. Nonetheless, because our sorter allows for polarization sorting, it allows for the execution of a QKD protocol in a dimension twice as great as that of a solely OAM based protocol. The ability to increase this dimension lowers the threshold on the quantum bit error rate needed to securely perform QKD, thus enabling the use of lower-quality sorters for this purpose. Improving the quality of this angular momentum sorter to that of its current OAM counterparts would also considerably enhance the performance of this QKD protocol to a level above those that solely rely on OAM. Namely, a device with a lower crosstalk would increase the quantum bit error rate which, in conjunction with a higher dimension, would also increase the protocol's secret key rate.

5. Conclusion

In conclusion, we fabricated the first device able to sort both orbital and spin optical angular momentum eigenstates using liquid crystal based PBOEs. The device's performance was first tested by feeding it with various circularly polarized beams with well-defined OAM values. We then verified that it could process beams in superpositions of optical angular momentum eigenstates into their respective sorted orders. We later calculated the crosstalk of our sorter's output and found that about 72% of a mode was confined within its assigned channel. Finally, we verified that our device could operate with single photons and exploited this feature to use it in a 10-dimensional BB84 QKD scheme. The performance of the latter, along with that of several other sorter-based applications, could be further improved by reducing the device's crosstalk. To achieve such a purpose, aberrations in the device must first be removed by improving its fabrication process. For instance, improvements could be made on the uniformity of the layers of materials coated on the device's glass substrate and on the uniformity of the cavity enclosing the liquid crystals. Likewise, more refined photo-alignment methods could also be beneficial [36]. Though this would significantly improve the sorter's quality, additional methods could also be employed to further reduce the device's crosstalk such as those that rely on the use of fan-out elements [10,11,37,38]. These can be added after the sorter's output or even be integrated within the PBOEs themselves. In comparison to other current OAM sorting devices, our system has both drawbacks and advantages. For example, the polarization-dependent nature of our phase elements prevents us from directly scaling down our scheme significantly. By comparison, a device akin to that presented in [12] with the addition of a polarization-dependent beam displacer would consist of a compactly configured three-element device that imparts less aberrations on the sorted beam.

The system presented here is a clear demonstration of simultaneous OAM and polarization sorting. Using state-of-the-art methods to produce high-quality liquid crystal elements [29,39–42] would increase the performance of our sorter to be on par with existing designs. With the

Optics EXPRESS

elimination of these technical limitations, our sorter benefits from several advantages. For instance, given that our PBOEs have a tunable half-wave condition and that our sorter's lenses are not integrated directly in the unwrapper and corrector elements, our sorting scheme can easily be adapted to other wavelengths. As implied by Eqs. (1, 2) this adaptation is feasible provided that λf maintains the same value as that of the sorter's original configuration. Moreover, both of our sorter's optical components, namely PBOEs and lenses, can be scaled down to ultra thin elements [43, 44]. Finally, the fact that our sorter relies on geometric phases makes it advantageous in applications that rely on similar processes. In particular, communications schemes employing vector vortex beams [45, 46] would benefit from our sorter given that these beams consist of a superposition of two components opposite in both OAM and circular polarization. Our device's antisymmetric sorting process would enable the sorting of vector vortex beams along adjacent positions and thereby simplify the analysis of the beam's vector vortex content. Such extensions to our methods would significantly improve the sorter's channel capacity and thereby its performance in applications such as classical super-dense coding and quantum communications.

Funding

Canada Research Chairs; Canada Excellence Research Chairs (CERC); Government of Canada; Natural Sciences and Engineering Research Council of Canada (NSERC).